Credit Author statement

Ji Zhang: Conceptualization, Methodology, Software, Validation, Formal analysis, Investigation, Resources, Data curation, Writing - original draft.

Xiaomeng Zhang: Conceptualization, Methodology, Software, Validation, Formal analysis, Investigation, Resources, Data curation, Writing - original draft.

Zhixiang Zhang: Software, Validation, Formal analysis.

PeilingZhou: Conceptualization, Methodology, Writing - review & editing, Supervision.

Yan Zhang: Methodology, Software.

Han Yuan: Conceptualization, Methodology, Validation, Formal analysis, Writing - review & editing, Supervision, Funding acquisition.

Performance improvement of ocean thermal energy conversion organic Rankine cycle under temperature glide effect

Ji Zhang[a,1], Xiaomeng Zhang[a1], Zhixiang Zhang[a], Peilin Zhou[b], Yan Zhang[a], Han Yuan[a*]

a. Marine Engineering, College of Engineering, Ocean University of China, 238 Songling Road, Laoshan district, Qingdao 266100, China

b. Department of Naval Architecture and Marine Engineering, University of Strathclyde, Glasgow G4 0LZ, United Kingdom

Corresponding author: Han Yuan

Phone/Fax: +86-532-66781105

E-mail: hanyuan@ouc.edu.cn

Address: 238 Songling Road, Laoshan district, Qingdao 266100, China

1: These authors contributed equally.

Abstract

The temperature glide effect of zeotropic mixtures on ocean thermal energy conversion (OTEC) cycle driven by a narrow temperature difference, which is significantly different from that in conventional low-grade energy technologies, is yet to be thoroughly studied. In this study, the binary zeotropic mixtures-based OTEC cycle is investigated. Comparative analysis of the classical zeotropic ORC and six types of zeotropic ORCs configured with or without series/parallel multi-pressure evaporators and single-/dual-outlet liquid-separated condensers were conducted. The results showed that zeotropic mixtures could be beneficial in ocean thermal energy conversion. Multi-pressure evaporation could significantly reduce the irreversible loss in the heat exchanger, and the series multi-pressure evaporator-based zeotropic ORC (SMZO) performed better than the parallel cycle (PMZO), with 0.09%–0.14% higher thermal

efficiency, 2.27%–3.11% higher turbine power output, and 0.89%–1.46% higher exergy efficiency. Liquid-separated condensation could improve the condensation effect by increasing the heat transfer coefficient, and liquid-separated dryness dominant the performance. Dual-outlet liquid-separated condensation could also increase cycle-levelised energy cost. Comparingly, the single-outlet liquid-separated condensation based cycle could reduce the levelised energy cost by 7.93% and 4.81%, respectively.

Keywords: OTEC; ORC; Zeotropic mixture; Multi-pressure evaporation; Liquid-separated condensation; Economic analysis

Graphical Abstract

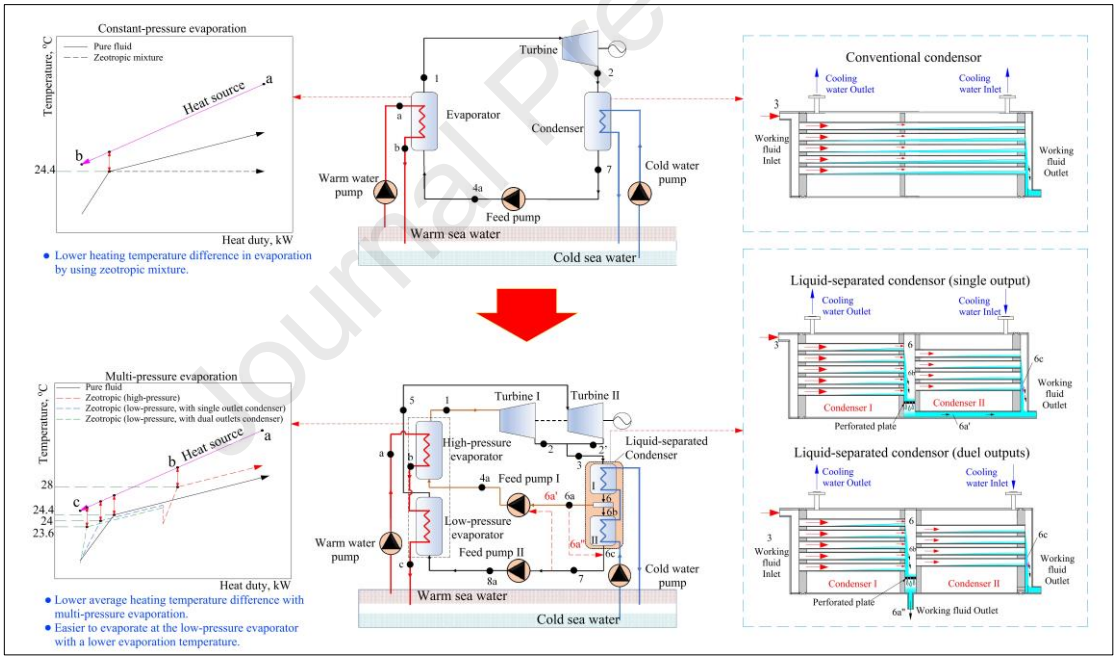

1. Introduction

Ocean thermal energy conversion (OTEC) technology uses surface warm seawater and deep cold seawater to drive a thermodynamic cycle and generate energy [1]. It is clean energy with huge reserves and stable quality. However, the OTEC cycle operates under a very small temperature difference of approximately 20–28 °C; therefore, the

energy conversion efficiency of the OTEC technology is very low [2], thus hindering its practical applications.

Considerable effort has been expended to improve the energy conversion efficiency of OTEC, and working fluid selection is an important method to this end. Ammonia [3] or an organic working medium [4, 5] is considered to be the ideal working fluid for the OTEC thermodynamic cycle because of its low boiling points. However, these working fluids experience isobaric and isothermal phase transitions during evaporation and condensation. The average heat transfer temperature difference between the heat/cold sources and the working fluid is much higher than the minimum heat transfer temperature difference [6, 7]. It is worth noting that zeotropic organic mixtures, in addition to ammonia/water, undergo variable-temperature evaporation or condensation under isobaric conditions, which is called the temperature glide [8]. This phenomenon can effectively improve the matching degree of the temperature curve between the working fluid and seawater; consequently, it can reduce the irreversibility in the evaporator and condenser, and increase the exergy efficiency of the organic Rankine cycle (ORC). Comparatively, the ammonia/water based cycle must involve a distillation process, and the enthalpy drop during the distillation will inevitably reduce the actual thermal efficiency of the cycle. Therefore, zeotropic organic mixtures promise greater potential in OTEC.

Currently, research on the zeotropic organic Rankine cycle (ZORC) focuses on the utilization of medium- and low- temperature waste heat, where the temperature of the heat source is much higher than that of the warm seawater, such as in solar power

generation, geothermal power generation, and waste heat recovery power systems [9-12]. However, effectively exploiting the advantages of the ZORC is faced with numerous challenges. One of them is how to better match the working fluid with the heat source. In general, the component type, component proportion, and working temperature range of the mixture in the two-phase zone together determine the temperature glide characteristics of the zeotropic working fluid, which in turn influences the cycle performance, but a larger temperature glide does not always lead to a higher cycle efficiency. Garg [13] found that zeotropic mixtures have significant differences in the amount of temperature glide under different constituent proportion ratios. Luo [14] compared the performance of six zeotropic working fluids at a heat source temperature range of 340–420K, and showed that the zeotropic working fluids, namely isopentane/hexane and isobutane/isopentane, whose temperature glide was higher than 5 K, had a significantly higher cycle performance than the zeotropic working fluids R245ca/R236ea and R245fa/R236ea, for which the temperature glide was lower than 5 K. Li [15] chose R227ea/R245ca as the working fluid to study the performance of a ZORC at a heat source temperature of 330—360 K; it was found that under the component proportion, for which the temperature glide reached a maximum, the output power of the cycle could not reach the peak. According to these studies, the temperature glide of the ZORC is beneficial for improving the cycle efficiency; however, it needs to meet the stringent conditions of the mixed working fluid constituent proportions.

In addition to adjusting the zeotropic component proportions, the multi-

evaporation method is deemed effective in improving the matching degree of the temperature curve between the working fluid and heat source. With this method, the evaporation process is decomposed into phase changes under different pressures and temperature ranges; therefore, the zeotropic working fluid can be divided into two parts, and the temperature difference in each part can be reduced. Guzović [16] compared the performance of the basic and dual-pressure ORC driven by a geothermal source of 373–453 K, and the dual-pressure ORC achieved a higher net power. Li [17] studied a two-stage evaporation ORC with two different configuration types for geothermal heat conversion and showed that with a geothermal water inlet temperature ranging from 363 to 390 K, the two-stage evaporation ORC reduced the irreversible loss. They also [18] investigated the applicable heat source temperatures of dual-pressure evaporation ORCs driven by heat sources operating at 373–473 K, and indicated that the applicable heat source temperature range generally increased as the working fluid critical temperature increased. In 2019, Li [19] studied a liquid-separated condensation-based ORC with a heat source temperature ranging between 373 and 473 K; it was found that the liquid-separated condenser was advantageous for the reduction in the condenser heat transfer area, and the specific investment cost of the ORC could be reduced by 4.6% over conventional condensation. The liquid-separated condenser is a new condensation heat transfer technology. It is mainly through gas-liquid separation to increase the quality of steam, reduce the heat transfer resistance of the condenser, and effectively improve the heat transfer coefficient of a non-azeotropic working medium at the condensing end. In 2021, Braimakis [20] compared the exergetic performance of a two-

stage ZORC, standard ORC, single-stage ZORC and two-stage pure fluid ORC, driven by the waste heat of 373 —433 K; it was found that the two-stage ZORC achieved the highest exergy efficiency between 373—413 K, while the single-stage ZORC achieved the highest exergy efficiency at 433 K.

In conclusion, the zeotropic mixture-based ORC has advantages in low-grade heat recovery for the temperature glide in evaporation and condensation processes. However, a traditional low-grade heat source is much higher than that of the warm seawater, and the applicability of zeotropic mixtures to OTEC remains unclear. On one hand, a high-temperature glide may not improve the performance of the thermal cycle; on the other hand, in OTEC cycle the temperature glide of the working fluid is limited within a very small range. The optimal cycle configuration and parameters for this narrow temperature difference still need to be investigated. Therefore, this study tries to reveal the effect of temperature glides of binary zeotropic mixtures on the OTEC cycle. A dry working fluid (R218), an isentropic working fluid (R125), and a wet working fluid (R143a) were selected as the components of the zeotropic mixture, and two representative zeotropic mixtures, R218/R125 and R218/R143a, were studied for OTEC. The thermodynamic and economic performances of a normal ZORC and six ZORCs configured with multi-pressure evaporators and a liquid-separated condenser were theoretically analyzed. The effects of the cycle structure, zeotropic mixture composition, and liquid-separation dryness on the cycle performance were explored.

2. OTEC cycle description

In this work, a normal ZORC and six ZORCs, configured with multi-pressure

evaporators and liquid-separated condenser were theoretically analyzed under OTEC working conditions; these include the ZORC (ZO), parallel multi-pressure evaporation ZORC (PMZO), series multi-pressure evaporation ZORC (SMZO), parallel multi-pressure evaporation ZORC with a single-outlet liquid-separated condenser (PMZO-SL), series multi-pressure evaporation ZORC with a single-outlet liquid-separated condenser (SMZO-SL), parallel multi-pressure evaporation ZORC with a dual-outlet liquid-separated condenser (PMZO-DL), and series multi-pressure evaporation ZORC with a dual-outlet liquid-separated condenser (SMZO-DL).

These OTEC cycles were all in organic Rankine form, major differences exist among them in the condensation and evaporation processes. As discussed, the liquid separation process was introduced to separate the condensed liquidus mixture within the condenser; on the other hand, the multi-pressure evaporation process was adopted to fit the multilevel pressure of the separated liquidus mixture, along with different ranges of evaporation temperature. A detailed cycle description is presented in the following sections.

2.1. Zeotropic ORC (ZO)

A schematic of the traditional ZORC (ZO)-based OTEC system is shown in Figure 1. This OTEC cycle comprises an evaporator, turbine, condenser, and pump. Warm sea water on the surface layer of oceans is utilized as the heating source to evaporate the working fluid, which flows into the turbine and produces power, while cold sea water beneath the ocean surface is utilized as the cooling source to condense the working fluid discharged from the turbine outlet.

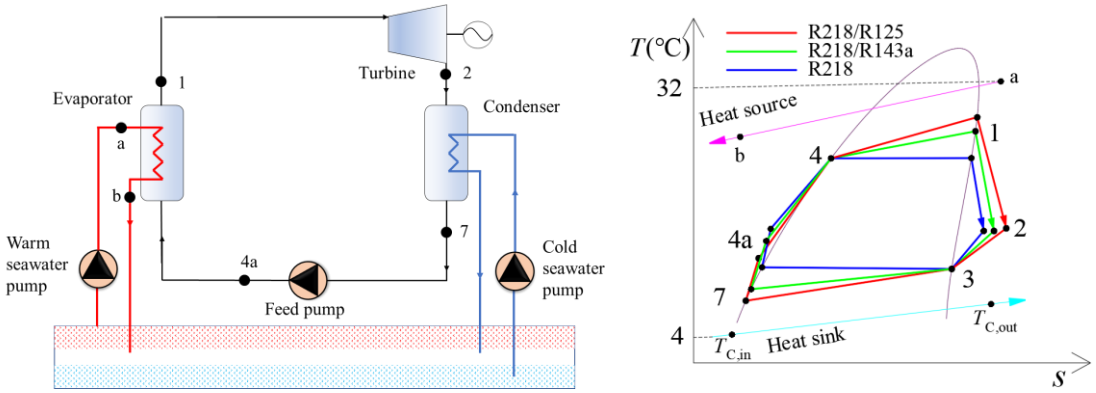

(a) (b)

Figure 1. Schematic of ZO-based ocean thermal energy conversion system: (a) ZORC; (b) corresponding *T*–*s* diagram.

2.2. Parallel or series multi-pressure evaporation ZORC (PMZO and SMZO, respectively)

Schematics of the parallel/series multi-pressure evaporation ZORC (PMZO/SMZO)-based OTEC systems are shown in Figure 2. In these two cycles, the condensed liquidus mixture is pumped into dual-pressure evaporators, in which different ranges of evaporation temperatures are maintained. Correspondingly, two turbines are introduced in parallel in the PMZO, and series in the SMZO. For the PMZO, the turbine outlet pressure remains the same at state points 2 and 2’; thus, the working fluid evaporated from the high-pressure and low-pressure evaporators drive the turbines separately, before mixing at the condenser inlet. For the SMZO, the outlet pressure of the first-stage turbine at state point 2 is equal to the inlet pressure of the second-stage turbine at state point 9, and the high-pressure working fluid drives the first-stage turbine to produce power, before mixing with the low-pressure working fluid, and driving the second-stage turbine. The *T*–*s* diagram reveals the difference in the expansion processes between these two cycles. The red line 7-4a-4-1-2 represents the heating and expansion

process of the zeotropic working fluid under high pressure; the blue line 7-8a-8-5-9-3 represents the heating and expansion process of the zeotropic working fluid under low pressure; and the black line 3-3'-7 represents the condensation process of the zeotropic working fluid in the condenser.

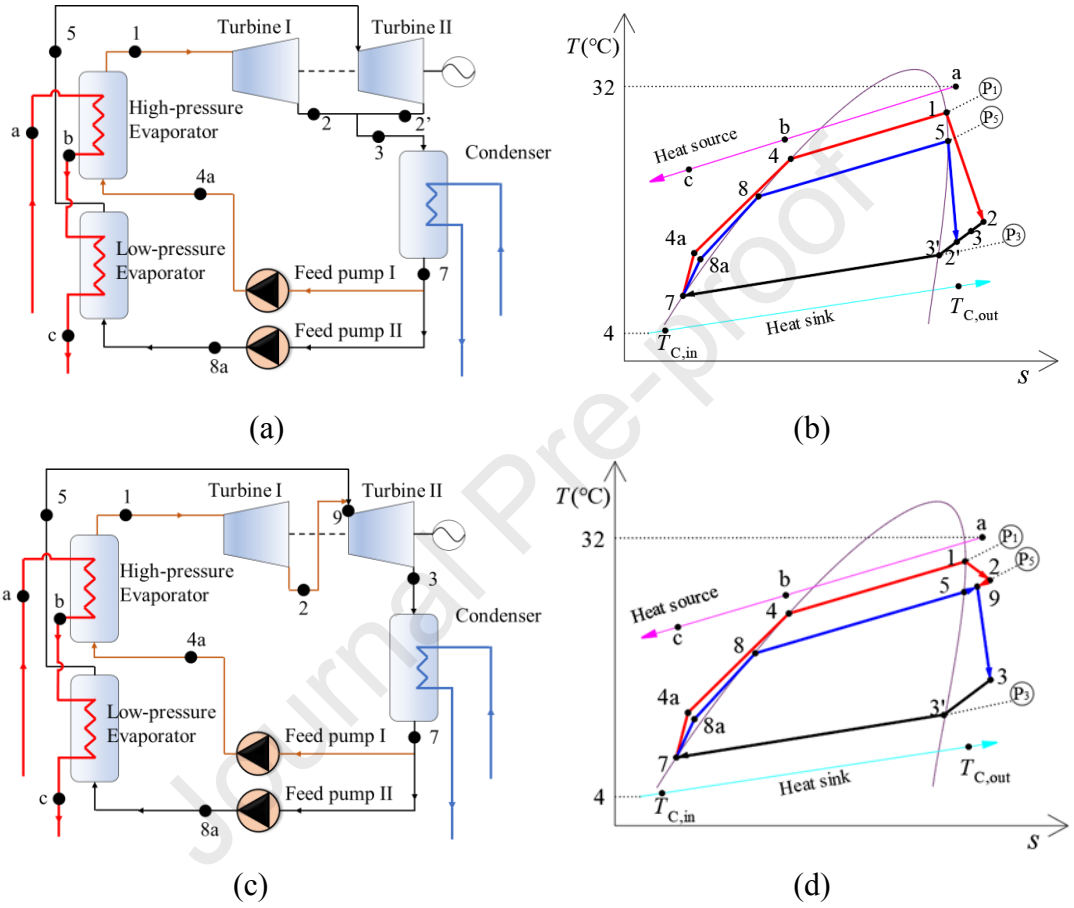

Figure 2. Schematics of the PMZO- and SMZO- based OTEC systems: (a) Schematic of the PMZO; (b) *T*–*s* diagram of the PMZO; (c) Schematic of the SMZO; (d) *T*–*s* diagram of the SMZO.

2.3. Parallel or series multi-pressure evaporation ZORC with a single-outlet liquid-separated condenser (PMZO-SL and SMZO-SL, respectively)

Schematics of the parallel/series multi-pressure evaporation ZORCs with a single-outlet liquid-separated condenser (PMZO-SL/SMZO-SL)-based OTEC systems are

shown in Figure 3. The two-stage evaporators and turbines are configured similarly in these cycles; however, the liquid-separated condensation process is introduced, and a schematic of the single-outlet liquid-separated condenser can be seen later in Figure 5. In the condenser, only one outlet is configured. The zeotropic vapor partly condenses into the liquidus mixture in the forepart of the condenser, which then gets separated in the middle part (at state point 6), thus leaving the vapor to condense sufficiently in the rear part. Through the liquid-separation method, the liquid on the inner surface of the heat exchanger pipe can be removed, and the condensation effect can be effectively improved. Finally, the liquid separated from the middle part mixes with the remaining condensed working fluid at the outlet (at state point 7). To demonstrate the thermodynamic processes, in Figure 3, the condenser is divided into two sections, namely, condenser I and condenser II, between which a separator is configured. The liquid-separated condensation processes of these two cycles are shown in the *T*–*s* diagram. The black lines 3-3'-6 and 6b-6c represent the condensation process of the zeotropic working fluid in the condenser.

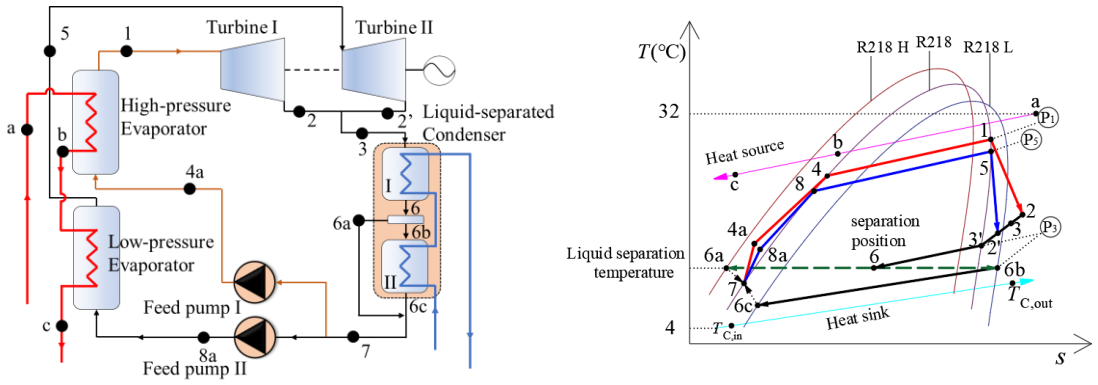

(a) (b)

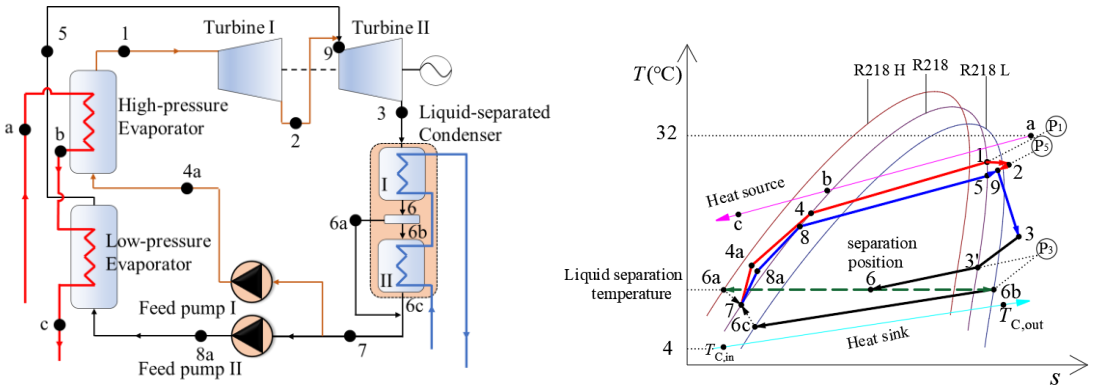

(c) (d)

Figure 3. Schematics of the PMZO-SL and SMZO-SL based OTEC systems: (a) Schematic of the PMZO-SL; (b) *T*–*s* diagram of the PMZO-SL; (c) Schematic of the SMZO-SL; (d) *T*–*s* diagram of the SMZO-SL.

2.4. Parallel or series multi-pressure evaporation ZORC with a dual-outlet liquid-separated condenser (PMZO-DL and SMZO-DL, respectively)

Figure 4 shows schematics of parallel/series multi-pressure evaporation ZORCs with a dual-outlet liquid-separated condenser (PMZO-DL/SMZO-DL)-based OTEC system. A schematic of the dual-outlet liquid-separated condenser can be seen later in Figure 5. In the above cycles, the liquid-separated condensation method is also introduced, wherein the liquidus mixture gets separated in the middle part (at state point 6a), which does not mix with the condensed mixture at the end, but is pumped back into the high-pressure evaporator directly. This means that the composition of the zeotropic organic working fluid in the high-pressure and low-pressure evaporators is no longer the same, and the temperature glide of the zeotropic working fluid is different. The liquid-separated condensation processes of these two cycles are shown in the *T*–*s* diagrams in Figure 4(b) and (d). The red line 6a-4a-4-1-2 represents the heating and expansion process of the zeotropic working fluid at high pressure, while the blue line

6c-8a-8-5-3 represents the same at low pressure.

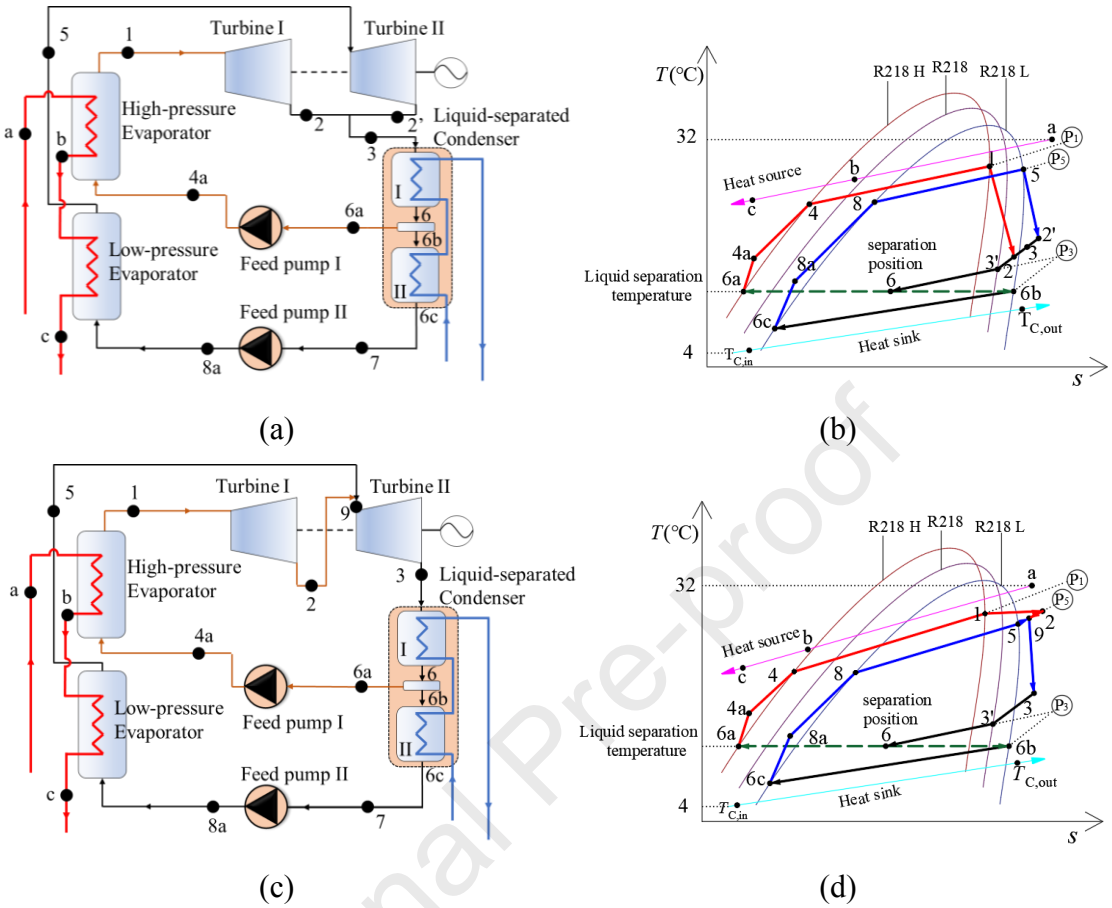

Figure 4. Schematics of PMZO-DL and SMZO-DL based OTEC systems: (a) Schematic of the PMZO-DL; (b) *T*–*s* diagram of the PMZO-DL; (c) Schematic of the SMZO-DL; (d) *T*–*s* diagram of the SMZO-DL.

2.5. Liquid-separated condenser

A schematic of the liquid-separated condenser is shown in Figure 5. The condenser is divided into two sections marked as condensers I and II by the gas-liquid separation metal laminates. As the zeotropic working fluid experiences gas-liquid separation at the junction, the film thickness of the working fluid in the tube is reduced; therefore, the heat transfer resistance of the condenser can be reduced, which ultimately increases the heat transfer coefficient of the condenser. Because the heat transfer coefficient and heat

transfer area of a heat exchanger are two variables with contrasting effects, the required heat transfer area of the heat exchangers of the ZORC can be decreased, thus leading to better economic performance.

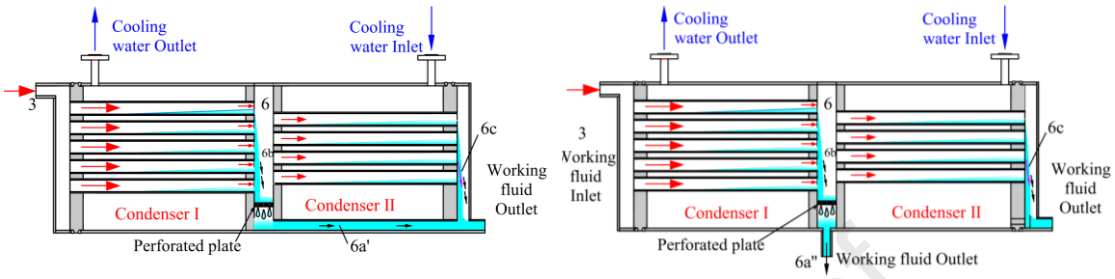

Figure 5. Schematics of the liquid-separated condenser: (a) single-outlet; (b) dual-outlet

Figure 5(a) shows the single-outlet liquid-separated condenser, Figure 5(b) shows the dual-outlet liquid-separated condenser. The main difference between the dual- and single- outlet modes is that the compositions of the zeotropic working fluids in the high-pressure and low-pressure evaporators are different, and the temperature glide in each evaporator is different.

2.6. Working fluid selection

In the ZORCs, the temperature glide needs to be controlled within a reasonable range, which can perfectly match the temperature drop at the heating/cooling seawater side. The theoretical performance of dual-pressure specific and liquid-separated condensation systems was mainly considered in this paper. The theoretical performance of the system and the isentropic characteristic of working medium determine the optional range of turbine outlet state, which is one of the most important factors affecting the circulation performance. Besides, the dry and wet characteristics of the

working fluids are important factors that can affect the expansion process of the ORC. Therefore, in this study, a dry working fluid (R218), an isentropic working fluid (R125), and a wet working fluid (R143a) were selected as the basic components of the zeotropic mixture. Two types of zeotropic mixtures, R218/R125 and R218/R143a, were studied. The properties of the zeotropic mixtures are summarised in Table 1. As the condensation temperature of R125 and R143a are very close (at -48.45 and -47.6 °C, respectively), the difference in the temperature glides between the zeotropic mixtures R218/R125 and R218/R143a is subtle. Therefore, the difference in the cycle performance caused by the temperature glides of these zeotropic mixtures can be eliminated. To more intuitively identify the fluid type of pure working medium, the temperature-entropy diagram of the specific pure working medium is shown in Figure 6.

Table 1. Properties of R218, R125, and R143a

Working fluid	T (°C)	T_c (°C)	P_c (MPa)	ODP	Safety	Fluid type
R218	–128	45.67	3.7	0	A1	Dry
R125	–48.45	66.05	3.6	0	A1	Isentropic
R143a	–47.6	73.1	3.6	0	A2	Wet

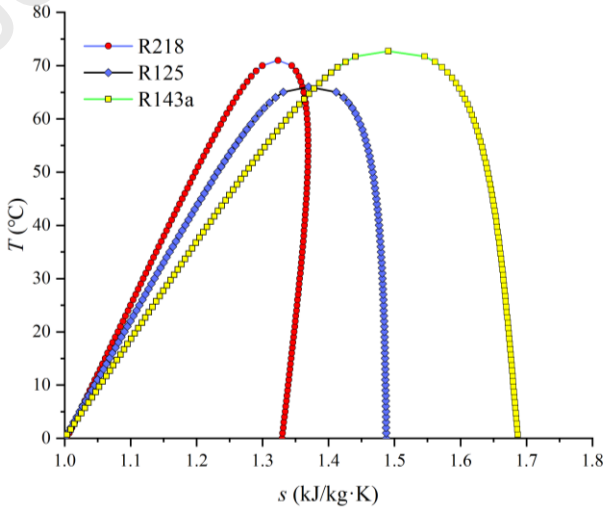

Figure 6. Dry and wet characteristics of R218, R125, and R143a.

The liquid-separated condenser plays an important role in the ZORCs. The effect of liquid-separated condensation on the component proportions of the selected

zeotropic mixtures in the condenser is shown in Figure 7. When the mass fraction of R218 in condenser I ($C_{CI,\,R218}$) was fixed, the higher the condensing dryness x, the closer the liquid separation position was to the inlet of condenser I. Moreover, at a high x, the mass fractions of R218 in condenser I ($C_{CI,\,R218}$) and condenser II ($C_{CII,\,R218}$) were close to each other. This is because a high x indicates that the zeotropic working fluid experiences a short condensing process in condenser I, and the change in the composition is not evident. Furthermore, when $C_{CI,\,R218}$ ranged between 0.6 and 0.8, x had a greater influence on $C_{CII,\,R218}$, which indicates that the impact of the liquid-separation position was complicated. The investigations on this impact are discussed in Sections 4 and 5.

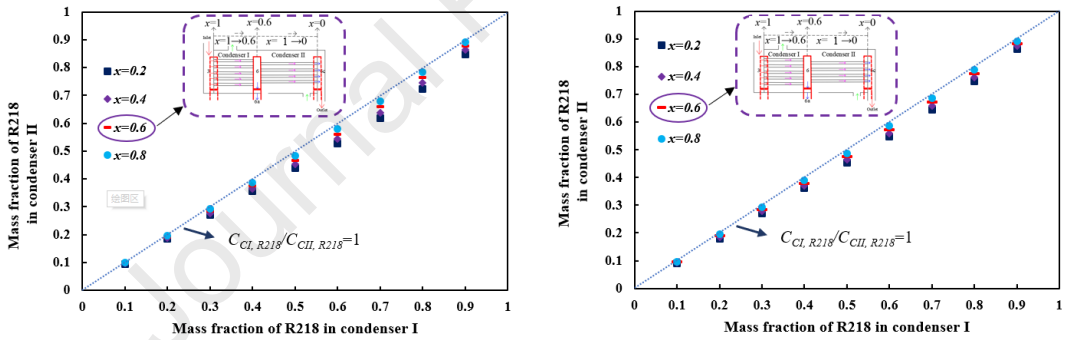

Figure 7. Variation of R218 mass fraction in the liquid-separated condenser for different liquid-separation dryness (x) values: (a) zeotropic mixture R218/R125; (b) zeotropic mixture R218/R143a

3. Model development

3.1. Modeling assumptions for simulation

The theoretical models of the OTEC cycles are established based on the following key assumptions:

- Each component of these cycles operates in a steady state.
- The pressure drops and heat losses in the evaporator, condenser, separator, and pipeline are not considered.
- The evaporator overheating and condenser undercooling are neglected.
- Liquidus mixture in a liquid-separated condenser is completely separated.
- The working fluid at the inlet of condenser □ is saturated.

3.2. Mathematical models of the thermodynamic cycles

The mathematical models for the OTEC cycles were established based on the first and second laws of thermodynamics. In addition, a radial-flow turbine model was introduced to determine the practical isentropic efficiency of the turbine. Moreover, a thermal economic model was established to evaluate the economic performance of these cycles.

3.2.1. Thermodynamic model

The mass and energy balance equation for each component is given as follows:

$$\sum m_{in} = \sum m_{out} \tag{1}$$

$$\sum m_{in} h_{in} + \sum m_{out} h_{out} + \sum Q_{in} - \sum Q_{out} + W = 0 \tag{2}$$

where m_{in} and m_{out} are the mass flow rates of the working fluid at the inlet and outlet of each component, respectively; h_{in} and h_{out} represent the enthalpy at the inlet and outlet of each component, respectively; Q_{in} and Q_{out} represent the heat input and output of each component, respectively; W represent the power.

The exergy conservation equation is given as:

$$Ex_Q + Ex_W + \sum m_{in} ex_{in} - \sum m_{out} ex_{out} = Ex_D \tag{3}$$

$$Ex_Q = (1 - \frac{T_0}{T})Q \tag{4}$$

$$Ex_W = W \tag{5}$$

$$ex = (h - h_0) - T_0(s - s_0) \tag{6}$$

$$Ex_{in} = m_{ws}((h_{E,in} - h_{E,out}) - T_0(s_{E,in} - s_{E,out})) \tag{7}$$

where Ex_Q is the exergy produced by heat transfer; Ex_W is the exergy produced by work; ex is the specific exergy; Ex_D is the exergy destruction; subscribe 0 represent reference state; $h_{E,in}$ and $s_{E,in}$ represent the enthalpy and entropy, respectively, of warm seawater at the inlet of the evaporator; and $h_{E,out}$ and $s_{E,out}$ represent the enthalpy and entropy, respectively, of the warm seawater at the outlet of the evaporator; m_{ws} represent the mass flow rate of warm seawater.

For the pump:

$$W_P = m_P(h_{P,out} - h_{P,in})\eta_P \tag{8}$$

$$ED_P = mT_0(s_{P,out} - s_{P,in}) \tag{9}$$

where W_P is the power consumption of the pump; $h_{P,out}$ and $s_{P,out}$ represent the enthalpy and entropy at the pump outlet, respectively; $h_{P,in}$ and $s_{P,in}$ represent the enthalpy and entropy at the pump outlet, respectively.

The net output power, thermal efficiency based on the first law of thermodynamics, and exergy efficiency based on the second law of thermodynamics are as follows:

$$W_{net} = W_t - W_P \tag{10}$$

$$\eta_{fir} = W_{net} / Q_E \tag{11}$$

$$\eta_{sec} = \frac{W_{net}}{Ex_{H,in}} \tag{12}$$

where W_{net} is the net output power; W_t is the turbine output power; Q_E is the evaporator heat input; η_{fir} is the thermal efficiency; $\eta_{\sec}$ is the exergy efficiency.

3.2.2. Turbine model

For the turbines, the radial-flow turbine model was used to determine the practical isentropic efficiency and exergy destruction.

The practical isentropic efficiency of the radial-flow turbine is

$$\eta_t = \eta_u - \xi_f - \xi_{le} \tag{13}$$

The peripheral efficiency of the radial-flow turbine is calculated as

$$\eta_u = \frac{u_1 c_{1u} - u_2 c_{2u}}{\Delta h_s} = 2(\overline{u}_1 \overline{c}_{1u} - \overline{u}_2 \overline{c}_{2u}) \tag{14}$$

The friction loss and leakage loss should also be considered when deriving the turbine's practical isentropic efficiency. These two losses are related to the working fluid properties and system operating conditions. The friction loss can be calculated as

$$\xi_f = f \frac{0.001287 \rho_1 u_1^{\ 3}}{Re_1^{\ 0.2} m_t \Delta h_s} D_1^{\ 2} \tag{15}$$

There is a tip clearance between the rotor blade tip and the shroud, which causes the leakage loss in the radial-inflow turbine. The leakage loss is defined as follows:

$$\xi_{le} = \begin{cases} 1.3\dfrac{\delta}{l_m}(\eta_u - \xi_f), & \dfrac{\delta}{l_m} \le 0.05 \\ (0.05 + 0.31\dfrac{\delta}{l_m})(\eta_u - \xi_f), & \dfrac{\delta}{l_m} > 0.05 \end{cases} \tag{16}$$

$$l_m = \left(l_1 + l_2\right)/2 \tag{17}$$

The meaning and initial value of parameters above please see the references of Song[21], and Pan and Wang[22].

3.2.3. Heat exchanger model

For the condensers of the PMZO-SL, PMZO-DL, SMZO-SL, and SMZO-DL, the composition of the working fluid is regulated by setting the position of the gas-liquid separation.

$$Q_{C,\mathrm{I}}=(m_{HP}+m_{LP})(h_3-h_6) \tag{18}$$

$$Q_{C,\mathrm{II}}=x(m_{HP}+m_{LP})(h_{6b}-h_{6c}) \tag{19}$$

$$ED_{C,\mathrm{I}}=T_0(m_{HP}+m_{LP})(s_6-s_3)+m_{CS}T_0(s_{C,out,x}-s_{C,in}) \tag{20}$$

$$ED_{C,\mathrm{II}}=T_0x(m_{HP}+m_{LP})(s_{6c}-s_{6b})+m_{CS}T_0(s_{C,out}-s_{C,out,x}) \tag{21}$$

$$T_6=T_{6b}=T_{6c} \tag{22}$$

$$P_6=P_{6b}=P_{6c} \tag{23}$$

where $Q_{C,\mathrm{I}}$ and $Q_{C,\mathrm{II}}$ are the condensation heat of condensers I and II, respectively; $ED_{C,\mathrm{I}}$ and $ED_{C,\mathrm{II}}$ are the exergy destructions of condensers I and II, respectively; h_6 and s_6 represent enthalpy and entropy at the condenser □ inlet; h_{6b} and s_{6b} represent enthalpy and entropy at the condenser □ inlet; h_{6c} and s_{6c} represent enthalpy and entropy at the condenser □ outlet; x is the dryness of the liquid at the liquid separation point; T_6 is the temperature at the dispensing point; P_6 is the pressure at the dispensing point; and $s_{C,out,x}$ represent the entropy of cold seawater at the outlet of condenser □.

The average heat transfer coefficient of each heat exchanger was calculated based on the energy balance and logarithmic heat exchange temperature difference of the heat exchanger.

$$\frac{1}{U_i}=\frac{1}{a_i}+\frac{\gamma_w}{\lambda_w}+\frac{1}{a_o} \tag{24}$$

$$A_i = \frac{Q_i}{U_i \Delta T_i} \tag{25}$$

$$\Delta T_i = \frac{\Delta T_{\max,i} - \Delta T_{\min,i}}{\ln(\frac{\Delta T_{\max,i}}{\Delta T_{\min,i}})} \tag{26}$$

$$A = \sum A_i \tag{27}$$

$$U = \frac{Q}{A \Delta T} \tag{28}$$

where U_i is the heat transfer coefficient of each section of the heat exchanger; a_i is the heat transfer coefficient of the working fluid in each section; a_o is the heat transfer coefficient at the warm seawater side of each section; γ_w is the tube wall thickness; λ_w is the thermal conductivity of the tube wall; A_i is the heat transfer area of each section; ΔT_i is the logarithmic heat exchange temperature difference of each section; A is the total heat transfer area; U is the average heat transfer coefficient; and $\Delta T_{\max,i}$ and $\Delta T_{\min,i}$ represent the maximum and minimum values, respectively of the heat transfer temperature difference between the seawater and working fluid in the heat exchanger.

The heat transfer coefficient in each heat exchanger was calculated as follows:

$$a = Nu \frac{\lambda}{d} \tag{29}$$

The Reynolds number was calculated as:

$$Re = \frac{ud}{\upsilon} \tag{30}$$

where λ is the thermal conductivity of the fluid; u is the flow rate in the tube; d is the diameter of the tube; and υ is the kinematic viscosity.

Using the correlation of Bernstein [23], the Nusselt number of the surface warm sea water and deep cold sea water flowing through the heat exchanger was calculated

as follows:

$$Nu = 0.3 + \frac{0.62 Re^{1/2} Pr^{1/3}}{[1+(0.4/Pr)^{2/3}]^{1/4}} [1 + (\frac{Re}{28200})]^{4/5} \quad (31)$$

In the preheating and desuperheating sections of these heat exchangers, the working fluid would experience a single-phase forced convection heat transfer. The Nusselt number was calculated based on the Gnielinski [24] correlation.

$$Nu = \frac{(f/8)(Re-1000)Pr}{1+12.7(f/8)^{1/2}(Pr^{2/3}-1)} \quad (32)$$

$$f = [0.79ln(Re) - 1.64]^{-2} \quad (33)$$

In the evaporator, the total heat transfer coefficient was approximately equal to the heat transfer coefficient of the gas side, which could be obtained using Kern's formula [25].

$$U_E = 0.36 \frac{\lambda_E}{d_E} Re_E^{0.55} Pr_E^{1/3} (\frac{\mu}{\mu_{WS}})^{0.14} \quad (34)$$

where μ is the dynamic viscosity of the working fluid and μ_{WS} is the dynamic viscosity of the warm seawater.

In the shell and tube type condenser, the Nusselt number of the pure working fluid was calculated following Shah [26] as

$$Nu_C = 0.023 Re_C^{0.8} Pr_C^{0.4} [(1-x)^{0.4} + \frac{3.8 x^{0.76} (1-x)^{0.04}}{Pr_C^{0.38}}] \quad (35)$$

In this study, the method proposed by Slive [27], and Bell and Ghaly [28] for calculating the condensation heat transfer coefficient for zeotropic mixtures was adopted, which is as follows:

$$\frac{1}{a_C} = \frac{1}{a_l} + \frac{Z_g}{a_g} \quad (36)$$

$$Nu_{C,g} = 0.023 Re_{C,g}^{0.8} Pr_{C,g}^{0.4} \tag{37}$$

$$Z_g = xC_p \frac{T_{C,g}}{h_{C,g}} \tag{38}$$

$$a_g = Nu_{C,g} \frac{\lambda_{C,g}}{d_{C,g}} \tag{39}$$

where a_C is the condensation heat transfer coefficient of the zeotropic mixture working fluid inside the condenser; a_l and is the condensation heat transfer coefficient of the liquid; a_g is the condensation heat transfer coefficient of gaseous steam; Z_g is the ratio of the sensible heat to the latent heat of the zeotropic mixture during the condensation process; and $h_{C,g}$ is the latent heat value of the zeotropic mixture during the condensation process.

3.2.4. Economic model

According to the configuration of the OTEC, the total cost of the cycle is mainly composed of the costs of the evaporator, condenser, turbine, working fluid pump, and seawater pump. The estimation of module cost of the OTEC system was adopted in this study, based on the economic evaluation model proposed in [29]. The purchased equipment cost (PEC) for each equipment module was calculated as follows:

$$PEC = 10^{(K_1 + K_1 \log_{10} Y + K_1 (\log_{10} Y^2))} \tag{40}$$

where Y represents each module of the heat exchanger area, turbine, feed pump, and seawater pump. The coefficients involved in the equipment module are fixed according to [30, 31].

The annual capital cost (ACC) was calculated as shown below:

$$ACC = 6.32 \sum_K PEC_K \cdot CRF \tag{41}$$

where *CRF* is the capital recovery rate. The coefficient 6.32 represents the additional cost associated with the purchased equipment costs [29, 32].

$$CRF = \frac{i(1+i)^n}{(1+i)^n - 1} \tag{42}$$

where i is the annual interest rate on the borrowed capital and n is the economic life of the cycle, which was set to 20 years in this study [33].

The annual operation and maintenance costs (*AOC*) were calculated as shown below:

$$AOC = 0.2\sum_K PEC_K \tag{43}$$

Finally, this study defined the thermal economy evaluation standard as the levelised energy cost (*LCOE*) [34, 35]:

$$LCOE = \frac{ACC + AOC}{\tau_{OH} \cdot W_{net}} \tag{44}$$

where τ_{OH} is the operating time. Considering natural disasters and various uncontrollable factors during actual operation, the operating time was set to 7000 h.

3.3. Solution procedure and initial assumptions

A program was developed using MATLAB to calculate the thermal performance of the cycles based on the established mathematical model. In this procedure, the thermophysical properties of the zeotropic mixtures were obtained from REFPROP [36] provided by NIST. Taking the PMZO-DL as an example, Figure 8 elaborates the solution steps. The initial parameters for the OTEC cycles are listed in Table 2.

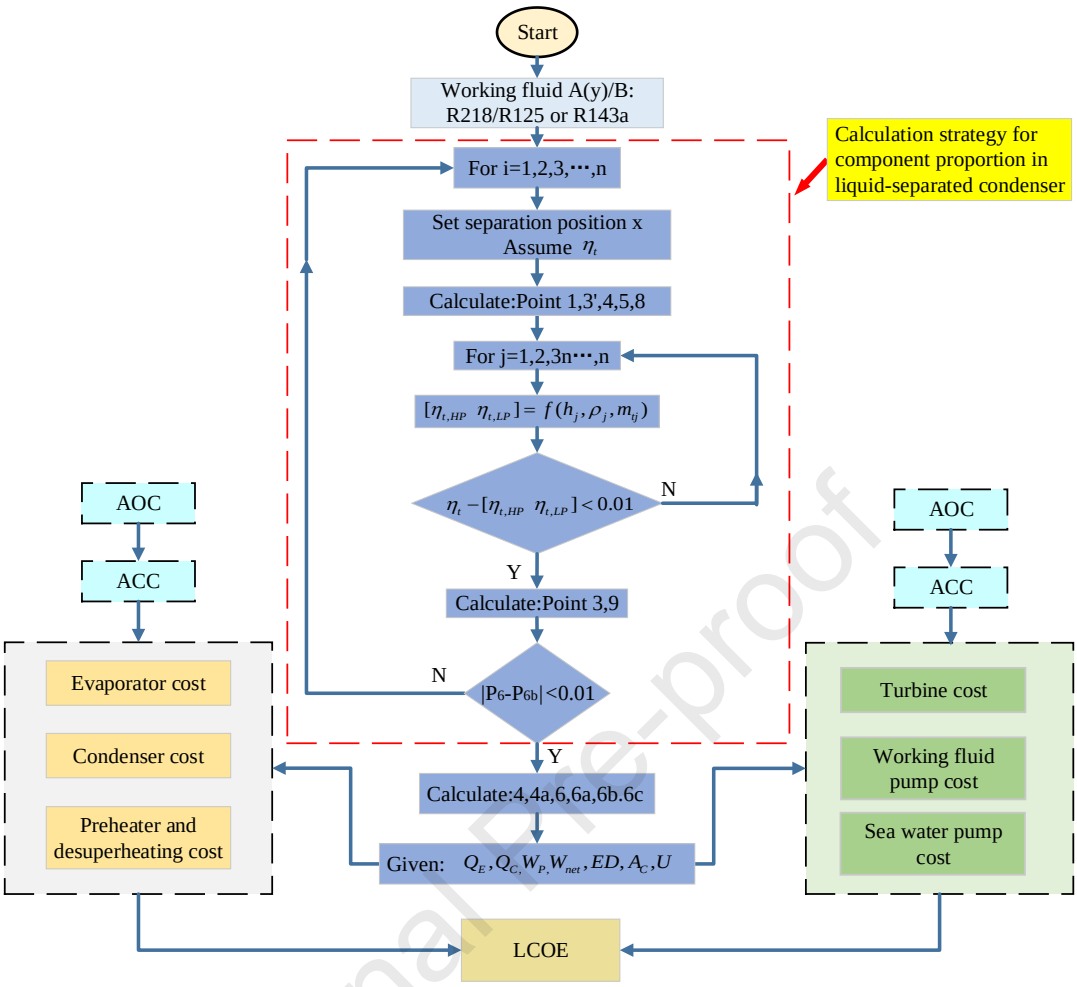

Figure 8. Program framework for PMZO-DL

Table 2. Initial parameters for the computations

Parameter	Value
Warm seawater inlet temperature, $T_{H,a}$ (°C)	32
Inlet temperature of the cooling water, $T_{C,in}$ (°C)	4
Mass flow rate of the working fluid, m (kg s^{-1})	1
Pinch point temperature difference of high-pressure evaporation, ΔT_{HP} (°C)	2
Pinch point temperature difference of low-pressure evaporation, ΔT_{LP} (°C)	2
Pinch point temperature difference of condenser, ΔT_C (°C)	2
Pump isentropic efficiency, η_P (%)	80
Ambient temperature, T_0 (°C)	20
Ambient pressure, P_0 (MPa)	0.1
Turbine velocity ratio, $\overline{u}_1$	0.72
Turbine nozzle velocity coefficient, φ	0.95
Turbine rotor blade velocity coefficient, ψ	0.95
Turbine degree of reaction, Ω	0.5

Turbine ratio of wheel diameter, $\overline{D}$ (m)	0.5
Turbine absolute velocity angle at the rotor inlet, θ_1 (°)	10
Turbine relative velocity angle at the rotor outlet, β_2 (°)	30
Tube wall thickness, γ_w (m)	0.02
Tube wall thermal conductivity, λ_w (W $m^{-1}K^{-1}$)	380
Annual loan interest rate, i (%)	4.9
Economic life of the cycle, n (year)	20
Operating time, τ_{OH} (h)	7000

For validation, the cases of the ZORC, multi-pressure evaporation and liquid-separated condensation system (LMZORC) were calculated with the present model based on validated data given in the published literature [37] and [14]. The initial parameters for the calculation were the same as those taken from the literature. According to the validation results summarized in Table 3 and Table 4.

Table 3. Validation results

Mixtures	***Mass fraction***	***η*/%**	**Source**
R227ea/R245fa	0.4/0.6	8.37	Ref. [37]
	0.4/0.6	8.411	Present
Butane/R245fa	0.1/0.9	8.18	Ref. [37]
	0.1/0.9	8.21	Present
R134a/R245fa	0.7/0.3	8.52	Ref. [37]
	0.7/0.3	8.54	Present

Table 4 Validation results with LMZORC model

Mixtures	***Mole fraction***	***W_{net}(kW)***	**Source**
Isopentane/hexane	0.92/0.08	404.06	Ref. [14]
	0.92/0.08	402.85	Present
Isobutane/isopentane	0.90/0.10	407.62	Ref. [14]
	0.90/0.10	404.19	Present
R245fa/R236ea	0.154/0.846	393.23	Ref. [14]
	0.154/0.846	392.54	Present

4. Performance analysis of OTEC cycles

In this study, the thermodynamic performance of two typical zeotropic mixture-based OTEC ORCs was studied. The detailed results and discussions are presented in

the following sections.

4.1. Thermodynamic performance of zeotropic working fluids

Two types of zeotropic mixtures (R218/R125 and R218/R143a) with different dry/wet characteristics were selected as the working fluids. Figure 9 shows the thermodynamic performance of the zeotropic mixture and pure mixture based OTEC-ORC. Considering the mass fraction of R218 as an independent variable, the performance of the cycles based on pure R218 (R218 mass fraction = 1), pure R125 or R143a (R218 mass fraction= 0), and zeotropic mixtures of R218/R125 and R218/R143a were obtained. With an increase in the R218 mass fraction in the mixture, both the thermal efficiency and exergy efficiency of the zeotropic cycles fluctuated, with a slight decrease at low R218 mass fractions, before reaching a peak with an R218 mass fraction of approximately 80% (or 0.8). Under the initial working conditions, the maximum cycle thermal efficiencies with R218/R125 and R218/R143a were 4.31% and 4.22%, respectively. Similarly, the maximum cycle exergy efficiencies reached 44.94% and 43.95%, respectively. In comparison, the thermal efficiencies of pure R218, R125, and R143a were 3.97%, 4.09%, and 4.20%, respectively, and the exergy efficiencies were 41.34%, 42.58%, and 43.80%, respectively. These results indicate that the zeotropic mixture-based OTEC-ORCs performed better in terms of energy conversion efficiency at a proper mass fraction of the working fluid.

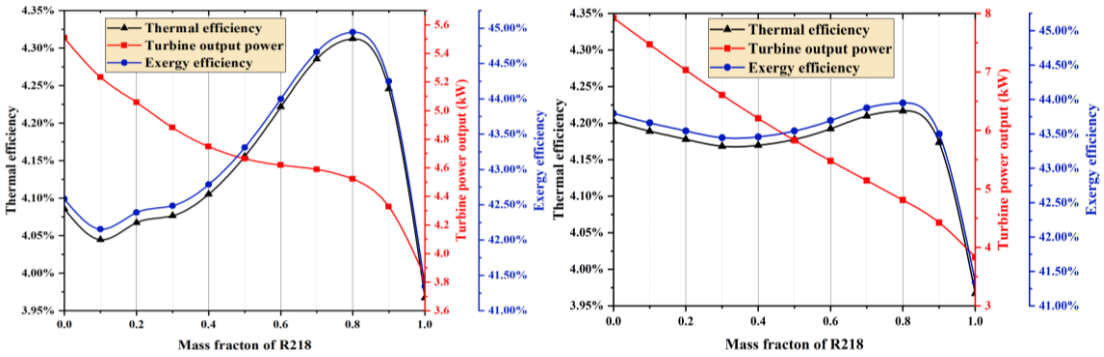

Figure 9. Thermal efficiency, turbine power output, and exergy efficiency of the ZORC versus mass fraction of R218 in two zeotropic mixtures: (a) R218/R125; (b) R218/R143a

In Figure 10, the evaporation and condensation pressures of R218/R125 and R218/R143a based cycles generally showed a downward trend as the R218 mass fraction in the mixed working fluid increased. The evaporation and condensation pressures of the zeotropic working fluid were between those of the corresponding mixtures of the two basic pure working fluids. Therefore, the mass fraction of R218 in the zeotropic working fluid mixture can be adjusted to meet the pressure requirements of the system. The evaporation temperature glides and condensation temperature glides of R218/R125-and R218/R143a based cycles first increased and then decreased with an increase in the R218 mass fraction in the zeotropic working fluid mixture. As a higher temperature glide results in a lower heat transfer temperature difference between the warm/cold seawater and the working fluid, and thus a lower irreversible loss, this result indicates that an optimal R218 mass fraction exists. Therefore, by choosing a proper mass fraction of the low boiling point working fluid R218, the irreversible losses of the zeotropic cycles can be reduced.

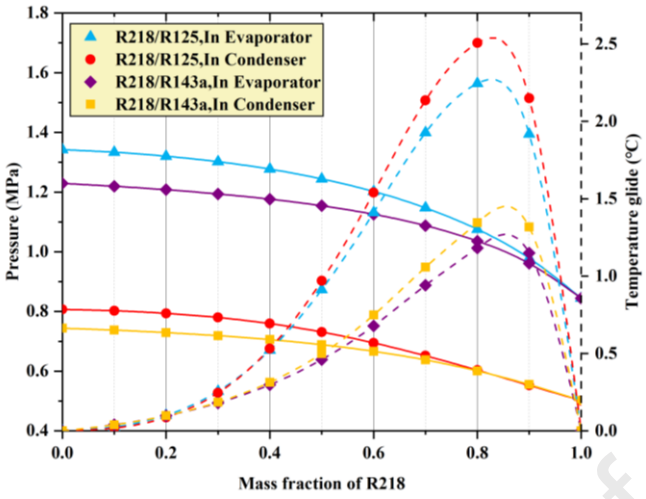

Figure 10. Temperature glide and pressure during evaporation and condensation of ZORCs versus mass fraction of R218

4.2. Performance comparison of ZORC and ORC

A comprehensive comparison of the cycle performances based on 10 types of azeotropic/zeotropic organic working fluids is presented in Figure 11. According to Figure 11(b), the turbine power outputs of the ZORCs were lower than those of the ORCs, because the low boiling point organics in the zeotropic mixtures would reduce the work capacity per unit working fluid, as shown in Figure 9. Nevertheless, the results shown in Figure 11(a) and (b) reveal that with the optimized mass fraction of the zeotropic mixture, the zeotropic ORCs could yield superior thermal and exergy efficiencies.

The thermodynamic performance of the ZORC was also compared with that from published studies [38-41] and the results are summarised in Table 5. Compared to the ORC, the ZORC had a remarkable advantage in terms of both thermal and exergy efficiencies. With similar initial assumptions, the R218/R125 based zeotropic cycle reached a thermal efficiency of 3.93% and an exergy efficiency of 36.38%. As the total

amount of ocean thermal energy is large, but the temperature difference is particularly small, the efficiency improvement of the ZORC is significant for OTEC.

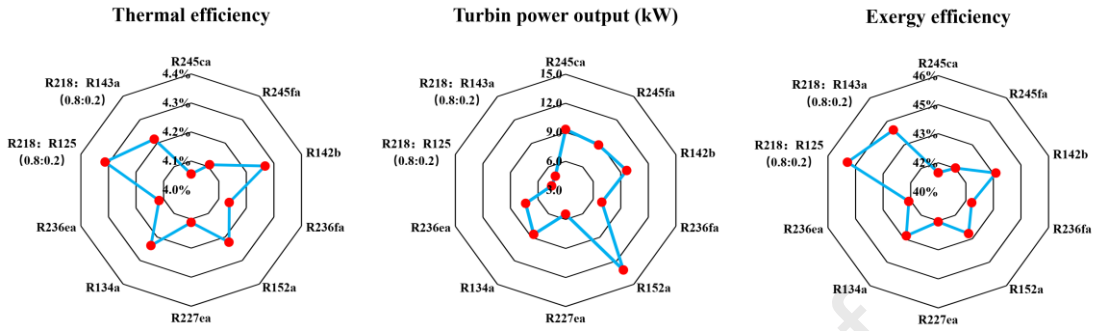

(a) (b) (c).

Figure 11. Performance comparison between ZORC and ORC: (a) thermal efficiency; (b) turbine power output; (c) exergy efficiency

Table 5. Performance comparison of OTEC cycles under similar initial working conditions

Theoretical	This study	Yang [38]	Meng [39]	Sun [40]	Vera [41]
Cycle type	Rankine	Rankine	Rankine	Rankine	Rankine
Working fluid	R218/R125 (0.8/0.2)	R600a	R601	R134a	R1234yf
Seawater inlet temperature (K)					
Warm	301	301	298.7	301	301
Cold	277	278	277.4	278	277
Component efficiency (%)					
Turbine	Calculated	90	80	85	82
Solution pump	80	80	80	85	80
Seawater pump	–	–	85	–	–
Thermal efficiency (%)	3.93	3.2	–	3.75	3.6
Exergy efficiency (%)	36.38	–	34.18	33	–

4.3. Performance comparison of PMZO and SMZO

Based on the results obtained in Figure 9 and 10, the optimal mass fraction of R218

for these ZORCs was approximately 0.8; therefore, the initial R218 mass fraction for all the configurations was fixed at 0.8. The mass flow rates in the high-pressure and low-pressure evaporators were both equal to 0.5 kg/s.

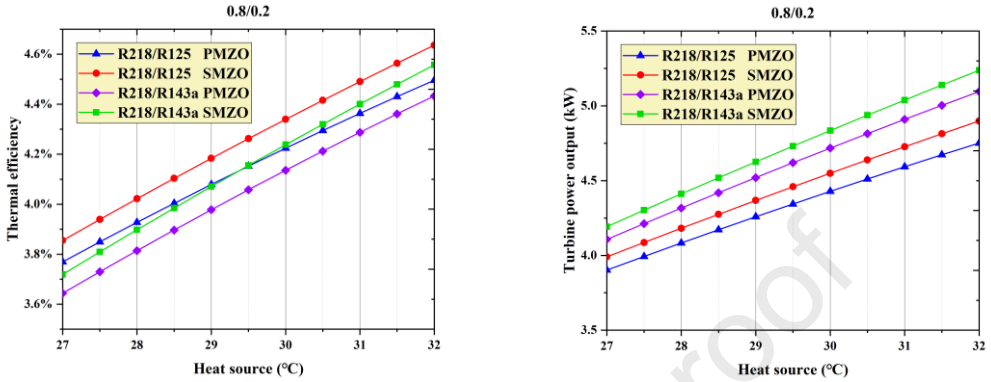

(a) (b)

Figure 12. Performance comparison of the PMZO and SMZO versus the warm seawater temperature

As shown in Figure 12, compared to the PMZO, the SMZO performed better, with 0.09%–0.14% higher thermal efficiency and 2.27%–3.11% higher turbine power output. In addition, the performances of the R218/R125 based cycles were better than those of the R218/R143a based cycles, which were similar to that of the ZORCs. As shown in Figure 12(a), when the inlet temperature of the heat source was higher than 30 °C, with the same mass fraction of R218, the thermal efficiency of the R218/R143a based SMZO was higher than those of the R218/R125 based PMZO. This result indicates that the change in the cycle structure type could compensate for the lack of thermophysical properties of the zeotropic working fluid.

4.4. Performance comparison of PMZO-SL, PMZO-DL, SMZO-SL, and SMZO-DL

As shown in Figure 13(a)–(c), when the dry working fluid R218/R125 zeotropic

mixture was used, the PMZO-SL, PMZO-DL, SMZO-SL, and SMZO-DL all reached their peak thermal and exergy efficiencies with an R218 mass fraction of 0.8. The SMZO-DL had the highest thermal and exergy efficiencies of 4.69% and 48.93%, respectively. As for the turbine power output, these cycles reached a peak with an R218 mass fraction of 0.1. According to Figure 13(d)–(f), when the wet working fluid R218/R143a zeotropic mixture was used, the PMLZO-SL reached a maximum thermal efficiency with an R218 mass fraction of 0.7, while the PMLZO-DL reached a maximum thermal efficiency with an R218 mass fraction of 0.1. It was found that a lower mass fraction of R218 resulted in a higher turbine power output.

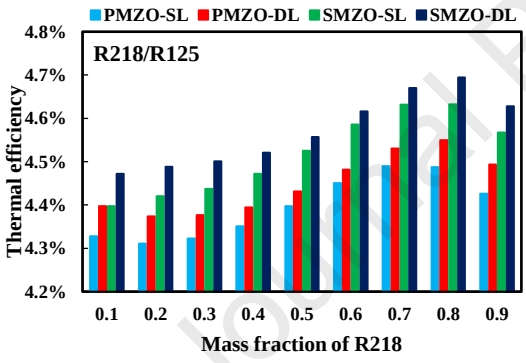

(a)

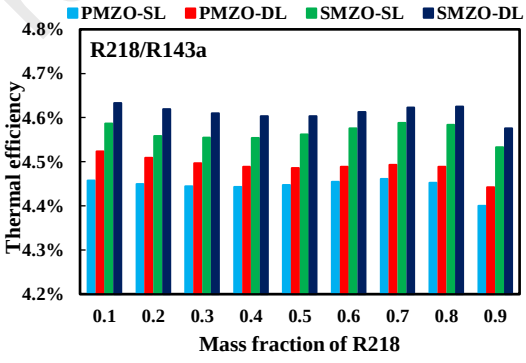

(d)

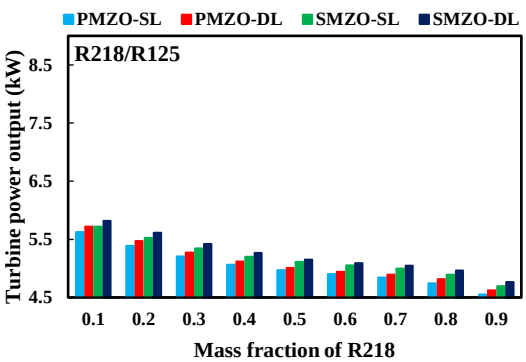

(b)

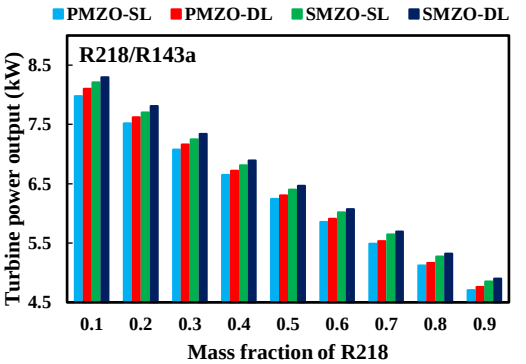

(e)

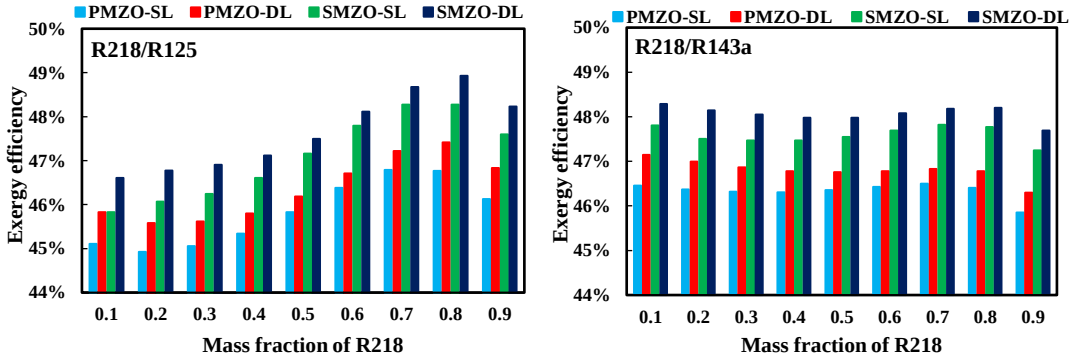

(c) (f)

Figure 13. Performance comparison of the PMZO-SL, PMZO-DL, SMZO-SL and SMZO-DL

Compared with the PMZO-SL and SMZO-SL, the efficiencies of the PMZO-DL and SMZO-DL were improved. This shows that the composition of the zeotropic working fluid in the high-pressure and low-pressure evaporators could be regulated by setting the liquid separation position in the condensation process such that the regulated zeotropic working fluid composition could match the heat absorption capacity of different working fluids and reduce the irreversible loss.

4.5. Analysis of irreversible loss for the ZO, SMZO, and SMZO-DL

Because of the temperature glide in the heat exchangers and regulation of the working fluid concentration in the liquid-separation condenser, the SMZO yielded a high efficiency in OTEC. Therefore, the SMZO and SMZO-DL were selected for irreversible loss analysis, and the results were compared with those of the ZO. The performances of the R218/R125-and R218/R143a based cycles were compared at the highest exergy efficiency with an 80% mass fraction of R218. Figure 14 shows the irreversible loss in each component and Figure 15 shows the detailed distribution of the irreversible loss. The results show that the SMZO-DL exhibited the lowest total

irreversible loss, followed by the SMZO and ZO. The irreversible loss of the turbines in the SMZO and SMZO-DL was slightly higher than that in the ZO cycle because the evaporation pressure of the dual-pressure evaporation was higher than that of the single-pressure evaporation; therefore, the average evaporation pressure of the turbine inlet was higher. In the SMZO and SMZO-DL, the irreversible loss of the working fluid pump was slightly higher than that of the ZO. The temperature at the turbine outlet (also the inlet of the condenser) would be higher due to the irreversible loss being converted into heat energy, which ultimately forced more heat to be exchanged in the condenser and caused the more irreversible loss. Compared with the ZO system, the irreversible loss of the SMZO-DL in the evaporator was reduced by 3.4% for the R218/R125 cycles and 2.4% for the R218/R143a cycles. The irreversible loss of the SMZO-DL in the evaporator was slightly lower than that in the SMZO. This indicates that the SMZO-DL could be made to match the temperature curve of the heat source better by adjusting the composition of the working fluid in the high-pressure and low-pressure evaporators.

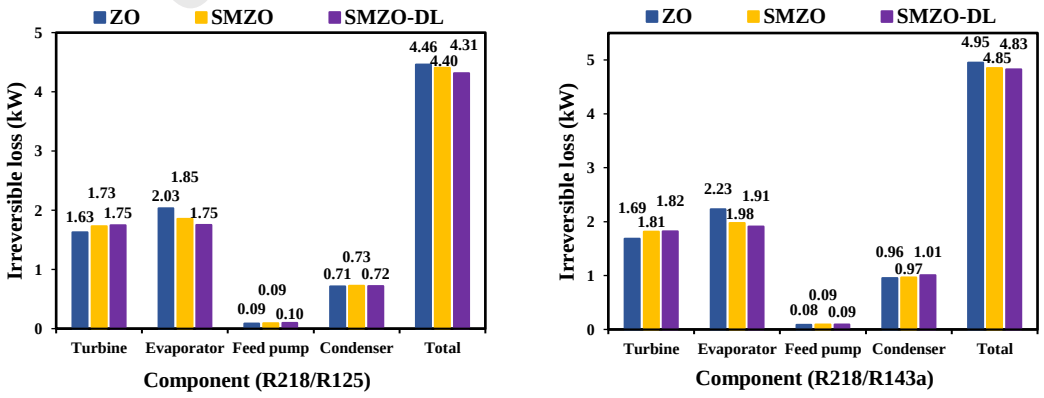

(a) (b)

Figure 14. Irreversible loss in each component: (a) R218/R125; (b) R218/R143a

According to Figure 15, for the R218/R125 cycles, the heat exchanger in the ZO

system accounted for approximately 61.57% (2.75 kW) of the total irreversible loss, and in the SMZO-DL system it accounted for 57.30% (2.47 kW) of the total irreversible loss. On the other hand, for the R218/R143a cycles, these proportions were 64.28% (3.17 kW) and 60.36% (2.92 kW). This shows that the multi-pressure evaporation and liquid-separated condensation processes could significantly reduce the irreversible loss in the heat exchanger.

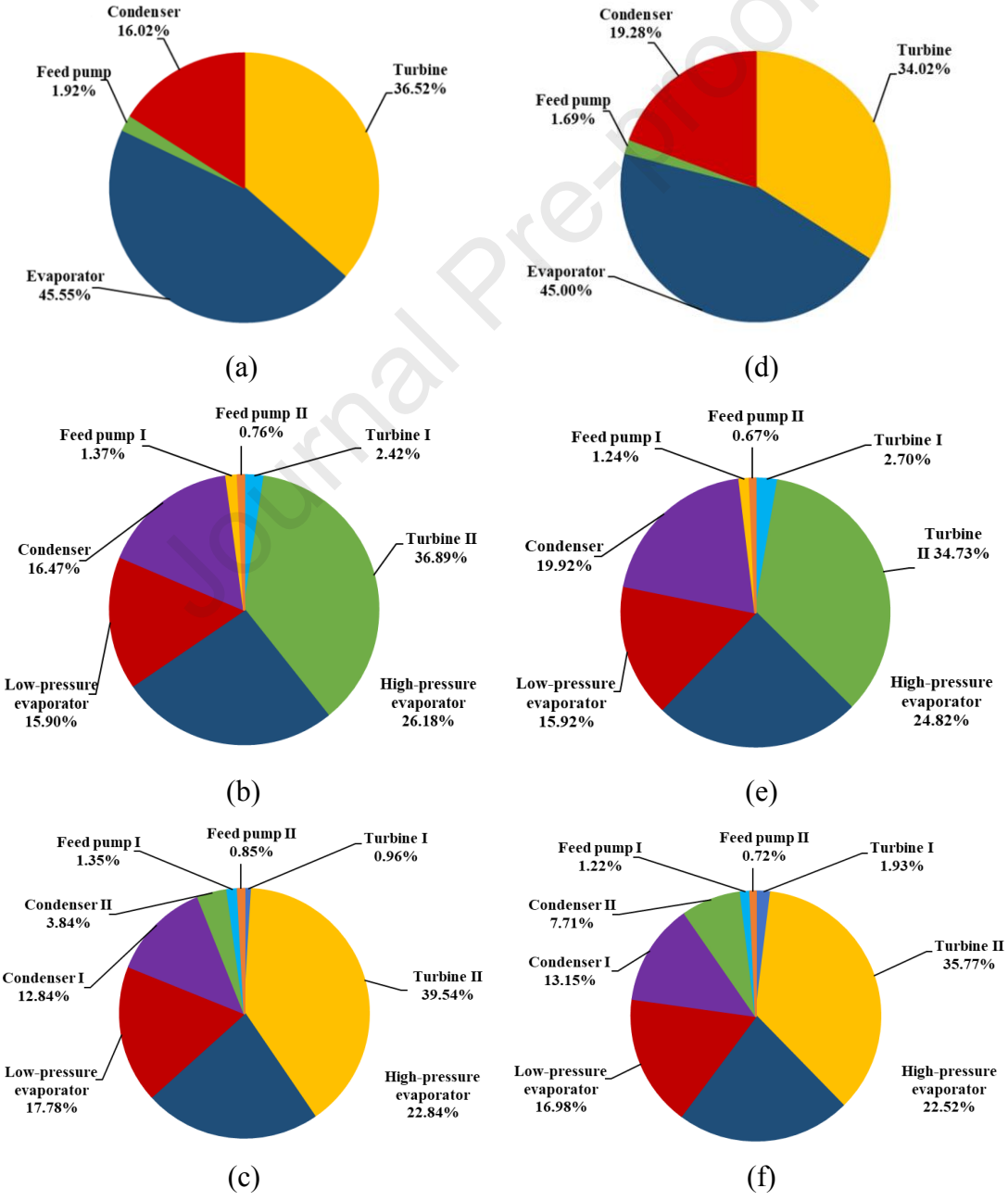

Figure 15. Distribution of irreversible losses: (a) ZO, R218/R125; (b) SMZO, R218/R125; (c) SMZO-DL, R218/R125; (d) ZO, R218/R143a; (e) SMZO, R218/R143a; (f) SMZO-DL, R218/R143a

Figure 16 shows the distribution of exergy destruction in the SMZO-DL. It was found that the evaporators, turbines, and condensers accounted for a major proportion. The exergy destruction in turbine II was much higher than that in turbine I; the reason for this is two-fold. On the one hand, the mass flow rate of turbine II was much higher, as the gaseous mixtures that evaporated from both the high-pressure and low-pressure evaporators flowed into turbine II; on the other hand, the practical efficiency of turbine II was much lower because of the relatively low pressure and temperature at the inlet of turbine II. In the cycle, 48.9% of the exergy product was obtained and could be further converted.

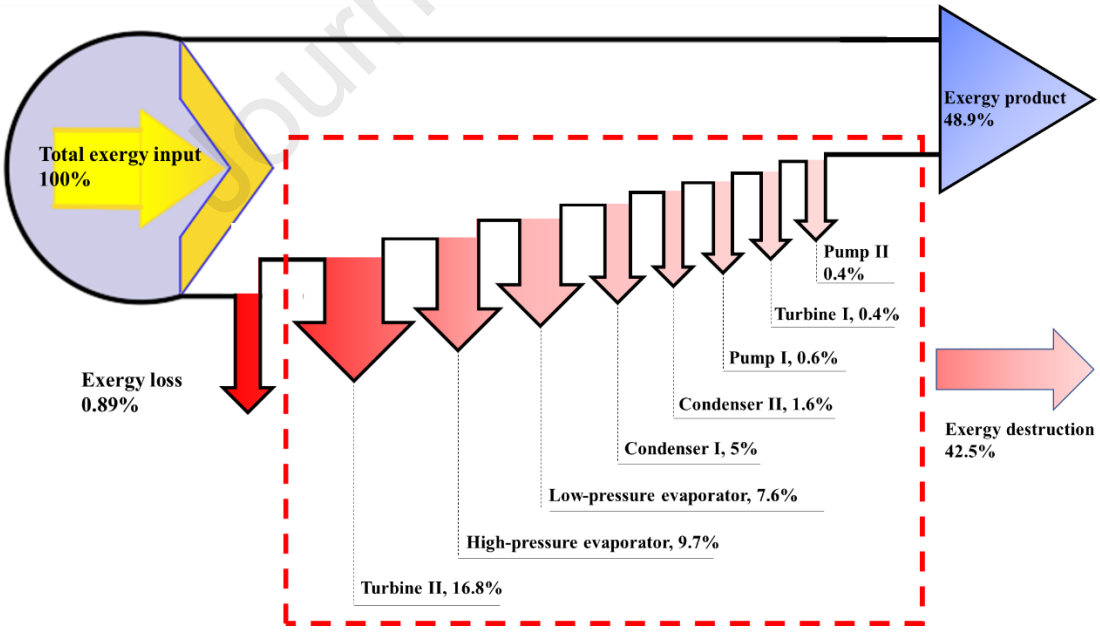

Figure 16. Exergy flow diagram for the SMZO-DL showing the exergy destruction in each component

4.6. Impact of liquid-separated condensation on cycle performance

Owing to the small temperature difference in the OTEC technology, the heat exchangers usually require an extremely large heat exchanger area, and account for a major share of the initial investment cost. From a comparison of the main performance indicators, such as thermal efficiency, turbine power output, and exergy efficiency of these zeotropic cycles, the liquid-separated condensation cycle showed a highly competitive efficiency in OTEC. Therefore, the impact of liquid-separated condensation on the average heat transfer coefficient and total heat transfer area of the condenser was conducted.

4.6.1. Average heat transfer coefficient of the condenser

Figure 17 shows the average condensation heat transfer coefficient with a variation of R218 mass fraction. When x was fixed, a lower R218 proportion in the zeotropic mixture led to a higher condensation heat transfer coefficient. Simultaneously, the R218/R125 based condenser had the lowest heat transfer coefficient at 80% R218 proportion. The thermal efficiency of the liquid-separated condensation cycles shown in Figure 13 reached a peak at R218 proportion of 80%. Thus, the liquid-separation method increased the thermal efficiency and decreased the heat transfer coefficient. Moreover, when x was 0.2, 0.4, 0.6, and 0.8, the heat transfer coefficient of the liquid-separated condenser reached a higher value compared to that of the conventional condensation. With a dryness of 0.4, the condensation heat transfer coefficient of the liquid-separated condenser increased by approximately 8.85%–28.14%. This indicates that liquid-separated condensation could effectively improve the condensation effect by enhancing heat transfer.

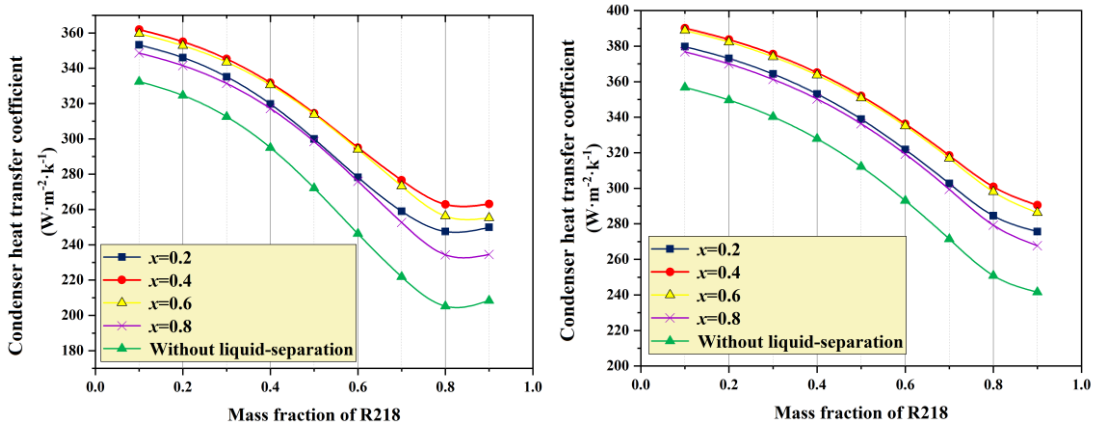

Figure 17. Heat transfer coefficient of liquid-separated condenser versus mass fraction of R218: (a) R218/R125; (b) R218/R143a

4.6.2. **Total heat transfer area of the condenser**

Figure 18 shows the variation in the condensation heat transfer area with the mass fraction of R218. It was found that with a fixed *x*, the heat transfer area for the R218/R125 based condenser first increased to a peak at 80% of R218 proportion and then decreased, with a further increase in the R218 proportion. However, for the R218/R143a based condenser, it showed a different trend; the heat transfer area decreased, in general, and increased slightly at 80% of R218 proportion. It is important to note that all the liquid-separated condensation with *x* values of 0.2.0.4, 0.6, and 0.8, drew a lower heat transfer area. Therefore, compared with conventional condensation, the liquid-separated condensation could significantly reduce the heat transfer area. This result is consistent with that shown in Figure 17. Also, with a dryness of 0.4, the condensation heat transfer area of the liquid-separated condenser was the lowest. This suggests that an appropriate *x* should be selected to reduce the area of the heat exchanger.

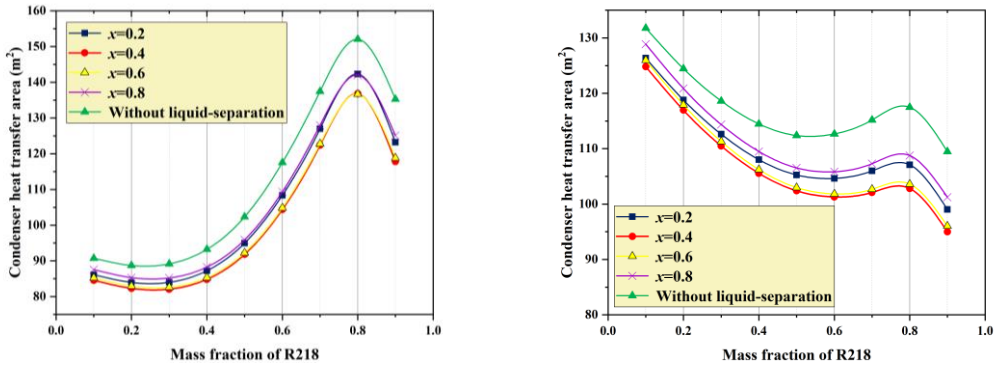

Figure 18. Heat transfer area of liquid-separated condenser versus mass fraction of R218: (a) R218/R125; (b) R218/R143a

4.7. Economic analysis

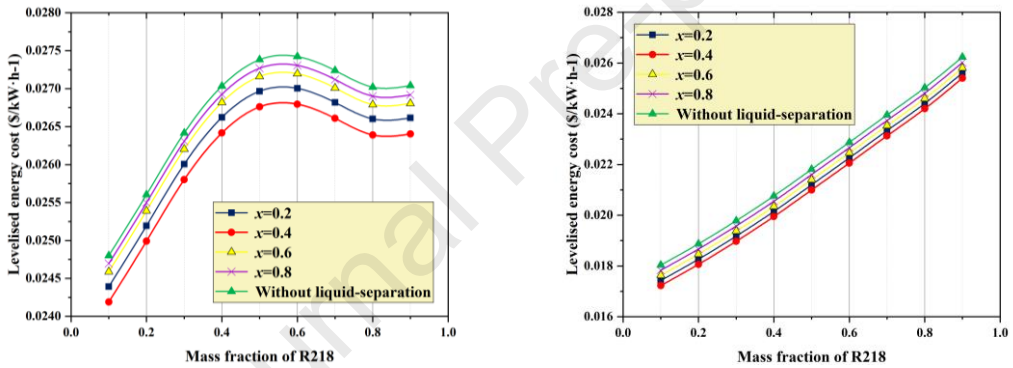

Figure 19. Levelised energy cost of the SMZO-SL-based OTEC system versus mass fraction of R218: (a) R218/R125; (b) R218/R143a

In this work, the partial pressure evaporation was set to cooperate with a non-azeotropic working medium, aiming at improving cyclic thermodynamic performance rather than the economy. The liquid-separated condensation was to obtain a smaller condensing heat transfer area, aiming at improving economic efficiency. The SMZO-SL based OTEC system was selected to conduct the economic analysis. The levelised energy cost of the OTEC system was obtained. In Figure 19, the levelised energy cost of the OTEC system fluctuated with a variation in the mass fraction of R218. For the

R218/R125 based system, the overall economic trend showed a peak at an R218 mass fraction of 80% regardless of whether the liquid-separated condensation was applied. This result can be compared with the results shown in Figure 12. When the R218 fraction was less than or equal to 0.3, the heat transfer area decreased slightly. Simultaneously, as shown in Figure 13, with a decrease in the R218 mass fraction, the turbine output work of the SMZO-SL cycle also decreased significantly. According to the mathematical model of the *LCOE*, the levelised energy cost increased. When the R218 mass fraction was greater than 0.3, and less than 0.6, the heat transfer area of the condenser gradually increased; however, the output work of this process still decreased with an increase in the R218 mass fraction; therefore, the levelised energy cost increased. Similarly, when the R218 mass fraction was greater than 0.6, the levelised energy cost showed a downward trend under the joint influence of the heat transfer area and turbine output work. Correspondingly, with a higher R218 mass fraction in the zeotropic R218/R143a working fluid, the overall system economy exhibited a decreasing trend. This means that although the heat transfer area increased for an R218 mass fraction of 0.5–0.8, the turbine output work decreased at the same time, resulting in a downward trend in the system-levelised energy cost. In addition, the results showed that the *x*-related separation position had a major influence on the levelised energy cost of the OTEC system. Regardless of the zeotropic mixture used, the levelised energy cost of the OTEC system was lower when the separation dryness was 0.4. By introducing liquid-separated condensation in the OTEC system, the levelised energy cost of the OTEC system could be reduced by 2.47% and 4.48%, respectively.

4.8. Performance comparison of cycles

The thermodynamic and economic performances of the ZO, PMZO, SMZO, PMZO-SL, PMZO-DL, SMZO-SL, and SMZO-DL are summarised in Table 6. Among these cycles, the SMZO-DL had the highest thermal efficiency, exergy efficiency, and turbine power output; these were, approximately 7.3%, 8.1%, and 8.3%, respectively higher than those of the ZO system with R218/R125, and 7.9%, 8.7%, and 8.8%, respectively higher than those of the ZO system with R218/R143a. These results indicate that the gas-liquid separation could effectively improve the thermal performance of the cycle. In addition, the thermal performance of the PMZO-SL was similar to that of the PMZO, and this was also the case with the SMZO-SL and SMZO. This suggests that for multi-pressure evaporation cycles, the single-outlet liquid-separated condensation did not improve the thermal performance further.

In addition, upon comparing the *LCOE* of each cycle, the PMZO-SL and SMZO-SL yielded a better economy of performance than the ZO. With the R218/R125 mixture, the levelised energy cost could be reduced by 7.93% and 7.86%, and with the R218/R143a mixture, it could be reduced by 4.81% and 4.70%, respectively. These results indicate that the increase in the equipment cost owing to multi-pressure evaporation did not reduce the thermal economy of the cycle. However, it is worth noting that the PMZO-SL and SMZO-SL were more economical than the PMZO-DL and SMZO-DL, which indicates that although the dual-outlet liquid-separated condensation method could improve the thermal performance, the overall economy of the OTEC system was reduced because of the higher equipment cost.

Table 6. Cycles performance comparison with same initial working condition

Working fluids	Cycle type	Optimal mole ratio	m(kg/s)	p_1 (MPa)	p_5 (MPa)	p_3 (MPa)	η_{fir}(%)	η_{sec}(%)	$W_{net}(kW)$	LCOE
R218/ R125	ZO	0.8:0.2	1	1.09	/	0.603	4.37	45.27	4.59	0.02864
	PMZO	0.8:0.2	1	1.17	1.08	0.603	4.49	46.78	4.74	0.02702
	SMZO	0.8:0.2	1	1.17	1.08	0.603	4.63	48.29	4.90	0.02702
	PMZO-SL	0.8:0.2	1	1.17	1.08	0.603	4.49	46.77	4.74	0.02637
	PMZO-DL	0.8:0.2	1	1.16	1.12	0.603	4.55	47.42	4.81	0.02813
	SMZO-SL	0.8:0.2	1	1.17	1.08	0.603	4.63	48.28	4.89	0.02639
	SMZO-DL	0.8:0.2	1	1.16	1.12	0.603	4.69	48.93	4.97	0.02813
R218/ R143a	ZO	0.8:0.2	1	1.05	/	0.601	4.28	44.35	4.89	0.02745
	PMZO	0.8:0.2	1	1.14	1.04	0.601	4.45	46.41	5.12	0.02503
	SMZO	0.8:0.2	1	1.14	1.04	0.601	4.58	47.78	5.27	0.02503
	PMZO-SL	0.8:0.2	1	1.14	1.04	0.601	4.45	46.40	5.12	0.02418
	PMZO-DL	0.8:0.2	1	1.13	1.06	0.601	4.49	46.78	5.17	0.02613
	SMZO-SL	0.8:0.2	1	1.14	1.04	0.601	4.58	47.77	5.27	0.02420
	SMZO-DL	0.8:0.2	1	1.13	1.06	0.601	4.62	48.20	5.32	0.02616
Initial paramters	a. T_4 and T_8 of PMZO, SMZO, PMZO-SL, PMZO-DL, SMZO-SL, and SMZO-DL are 28□ and 24□, respectively.									
	b. T_4 of ZO are 24.4□ for R218/R125 ; T_4 of ZO are 24.41□ for R218/R143a.									
	c. T_3 of ZO, PMZO, SMZO, PMZO-SL, PMZO-DL, SMZO-SL, and SMZO-DL are 6□.									
	d. m_{HP} and m_{LP} of PMZO, SMZO, PMZO-SL, PMZO-DL, SMZO-SL, and SMZO-DL are 0.6 kg/s and 0.4 kg/s, respectively.									

5. Conclusions

This study investigated the performance of ZORCs for OTEC. A dry working fluid (R218), an isentropic working fluid (R125), and a wet working fluid (R143a) were selected as the components of the zeotropic mixtures, and two representative zeotropic mixtures, R218/R125 and R218/R143a, were studied. The thermodynamic and economic performances of a normal ZORC and six ZORCs, configured with multi-pressure evaporators and a liquid-separated condenser, were theoretically analysed. The influence of the cycle structure, zeotropic mixture composition, and liquid-separation dryness on the cycle performance was studied. The main conclusions are as follows:

1) With the temperature glides in evaporation and condensation, the zeotropic mixture-based OTEC-ORC performed better than conventional OTEC-ORC in

terms of energy conversion efficiency. For zeotropic mixtures R218/R125 and R218/R143a, the optimal mass fraction of R218 was 80%.

2) The multi-pressure evaporation processes can reduce the irreversible loss in the heat exchanger. Compared with the PMZO, SMZO performed better, with 0.09%–0.14% higher thermal efficiency, 2.27%–3.11% higher turbine power output, and 0.89%–1.46% higher exergy efficiency, with the warm seawater temperature ranging within 27–32 °C and cold seawater temperature at 4°C.

3) The liquid-separated condensation can effectively improve the condensation effect by increasing the heat transfer coefficient. With the optimised dryness at 0.4, the condensation heat transfer coefficient of the liquid-separated condenser increased by approximately 8.85%–28.14%.

4) Compared with the single-outlet liquid-separated condensation process, the dual-outlet liquid-separated condensation process could improve the cycle thermal performance by 0.87%-2.23%; however, it also increased the cycle-levelised energy cost by 6.67%-8.10%.

5) The single-outlet liquid-separated condensation did not affect the cycle thermal performance improvement; nevertheless, it could effectively increase the cycle economic performance. With R218/R125 and R218/R143a mixtures, the levelised energy cost of PMZO-SL could be reduced by 7.93% and 4.81%, respectively.

Acknowledgment

The authors acknowledge the support provided by the National Natural Science

Foundation of China (51706214), the Key Technology Research and Development Program of Shandong (2017GHY15113) and Natural Science Foundation of Shandong (ZR2020me186).

References

[1] Kim NJ, Ng KC, Chun W. Using the condenser effluent from a nuclear power plant for Ocean Thermal Energy Conversion (OTEC). International Communications in Heat & Mass Transfer 2009;36:1008-1013.

[2] Yuan H, Mei N, Hu S, Wang L, Yang S. Experimental investigation on an ammonia-water based ocean thermal energy conversion system. Appl Therm Eng 2013;61:327-333.

[3] Yoon JI, Son CH, Baek SM, Ye BH, Kim HJ, Lee HS. Performance characteristics of a high-efficiency R717 OTEC power cycle. Appl Therm Eng 2014;72:304-308.

[4] Faizal M, Ahmed MR. Experimental studies on a closed cycle demonstration OTEC plant working on small temperature difference. Renew Energ 2013;51:234-240.

[5] Bernardoni C, Binotti M, Giostri A. Techno-economic analysis of closed OTEC cycles for power generation. Renew Energ 2019;132:1018-1033.

[6] Etemoglu AB. Thermodynamic investigation of low-temperature industrial waste-heat recovery in combined heat and power generation systems. International Communications in Heat & Mass Transfer 2013;42:82-88.

[7] Chen H, Goswami DY, Stefanakos EK. A review of thermodynamic cycles and working fluids for the conversion of low-grade heat. Renewable and Sustainable Energy Reviews 2010;14:3059-3067.

[8] Abadi GB, Kim KC. Investigation of organic Rankine cycles with zeotropic mixtures as a working fluid: Advantages and issues. Renew Sust Energ Rev 2017;73:1000-1013.

[9] Modi A, Haglin D F. A review of recent research on the use of zeotropic mixtures in power generation systems. Energy Conversion & Management 2017;138:603-626.

[10] Angelino G, Paliano P. Multicomponent Working Fluids For Organic Rankine Cycles (ORCs). Energy 1998;23:449-463.

[11] Chen H, Goswami DY, Rahman MM, Stefanakos EK. A supercritical Rankine cycle using zeotropic mixture working fluids for the conversion of low-grade heat into power. Energy 2011;36:549-555.

[12] Lu P, Luo X, Wang J, Chen J, Liang Y, Yang Z, et al. Thermo-economic design, optimization, and evaluation of a novel zeotropic ORC with mixture composition adjustment during operation - ScienceDirect. Energ Convers Manage 2021;230.

[13] Garg P, Kumar P, Srinivasan K, Dutta P. Evaluation of isopentane, R-245fa and their mixtures as working fluids for organic Rankine cycles. Appl Therm Eng 2013;51:292-300.

[14] Luo X, Huang R, Yang Z, Chen J, Chen Y. Performance investigation of a novel zeotropic organic Rankine cycle coupling liquid separation condensation and multi-pressure evaporation. Energy Conversion & Management 2018;161:112-127.

[15] Li Z, Bao J. Thermodynamic analysis of organic Rankine cycle using zeotropic mixtures. Appl Energ 2014;130:748-756.

[16] Guzovic Z, Raskovic P, Blataric Z. The comparision of a basic and a dual-pressure ORC (Organic

Rankine Cycle): Geothermal Power Plant Velika Ciglena case study. Energy 2014;76:175-186.

[17] Li T, Zhang Z, Jian L, Yang J, Hu Y. Two-stage evaporation strategy to improve system performance for organic Rankine cycle. Appl Energ 2015;150:323-334.

[18] Li J, Ge Z, Duan Y, Yang Z, Liu Q. Parametric optimization and thermodynamic performance comparison of single-pressure and dual-pressure evaporation organic Rankine cycles. Applied Energy -Barking Then Oxford- 2018;217:409-421.

[19] Li J, Hu S, Yang F, Duan Y, Yang Z. Thermo-economic performance evaluation of emerging liquid-separated condensation method in single-pressure and dual-pressure evaporation organic Rankine cycle systems. Appl Energ 2019;256:113974.

[20] Braimakis K, Grispos V, Karellas S. Exergetic efficiency potential of double-stage ORCs with zeotropic mixtures of natural hydrocarbons and CO2. Energy 2021;218.

[21] Song J, Gu CW, Ren X. Influence of the radial-inflow turbine efficiency prediction on the design and analysis of the Organic Rankine Cycle (ORC) system. Energ Convers Manage 2016;123:308-316.

[22] Pan L WH. Improved analysis of Organic Rankine Cycle based on radial flow turbine. Appl Therm Eng 2013;61:606-615.

[23] Churchill SW, Bernstein M. A Correlating Equation for Forced Convection From Gases and Liquids to a Circular Cylinder in Crossflow. Asme Transactions Journal of Heat Transfer 1977;99:300-306.

[24] Zhang S, Wang H, Guo T. Performance comparison and parametric optimization of subcritical Organic Rankin Cycle (ORC) and transcritical power cycle system for low-temperature geothermal power generation. Appl Energ 2011;88:2740-2754.

[25] Kern, DonaldQuentin. Process heat transfer /-1st ed: Process heat transfer /-1st ed; 1950.

[26] Shah MM. A general correlation for heat transfer during film condensation inside pipes. Int J Heat Mass Tran 1979;22:547-556.

[27] Silver RS. An approach to a general theory of surface condensers. ARCHIVE Proceedings of the Institution of Mechanical Engineers 1847-1982 (vols 1-196) 1963;178:339-376.

[28] Bell J, Ghaly A. An approximate generalized design method for multicomponent/partial condensers. AIChE Symp 1973.

[29] Li G. Organic Rankine cycle performance evaluation and thermoeconomic assessment with various applications part I: Energy and exergy performance evaluation. Renew Sust Energ Rev 2016;53:490-505.

[30] Turton RJ. Analysis, Synthesis and Design of Chemical Processes:United States Edition. Prentice-Hall international series in the physical and chemical engineering sciences 2012.

[31] Turton R, Bailie RC, Whiting WB. Analysis, synthesis and design of chemical processes. 2003.

[32] Algieri A, Morrone P. Techno-economic Analysis of Biomass-fired ORC Systems for Single-family Combined Heat and Power (CHP) Applications. Energy Procedia 2014;45:1285-1294.

[33] Zhang C, Liu C, Wang S, Xu X, Li Q. Thermo-economic comparison of subcritical organic Rankine cycle based on different heat exchanger configurations. Energy 2017;123:728-741.

[34] Basaran A, Ozgener L. Investigation of the effect of different refrigerants on performances of binary geothermal power plants. Energy Conversion & Management 2013;76:483-498.

[35] Shu G, Liu L, Hua T, Wei H, Xu X. Performance comparison and working fluid analysis of subcritical and transcritical dual-loop organic Rankine cycle (DORC) used in engine waste heat recovery. Energy Conversion & Management 2013;74:35-43.

[36] Lemmon EW, Huber ML, Mclinden MO. NIST Standard ReferenceDatabase 23: Reference Fluid

Thermodynamic and Transport Properties-REFPROP. 9.0. NIST NSRDS - 2010.

[37] Lijun Y, Yadong Z, Yuandan W. Medium and low temperature waste heat power generation technology: Shanghai Jiaotong University Press; 2015.

[38] Yang MH, Yeh RH. Analysis of optimization in an OTEC plant using organic Rankine cycle. Renew Energ 2014;68:25-34.

[39] A MW, A RJ, B HZ, A CM, A NL, A YZ. An innovative Organic Rankine Cycle (ORC) based Ocean Thermal Energy Conversion (OTEC) system with performance simulation and multi-objective optimization. Appl Therm Eng 2018;145:743-754.

[40] Sun F, Ikegami Y, Jia B, Arima H. Optimization design and exergy analysis of organic rankine cycle in ocean thermal energy conversion. Appl Ocean Res 2012;35:38-46.

[41] Vera D, Baccioli A, Jurado F, Desideri U. Modeling and optimization of an ocean thermal energy conversion system for remote islands electrification. Renew Energ 2020;162.

Highlights

- Binary zeotropic based ORC for OTEC between 27–32 °C and 4 °C is studied.
- Multi-pressure evaporators and liquid-separated condenser are configurated.
- Optimized composition of R218/R125 and R218/R143a are obtained.
- Thermal efficiency of SMZO-DL can increase by 7.3%-7.9% than ZO system.
- Levelised energy cost of PMZO-SL could be reduced by 4.81%-7.93% than ZO system.

Nomenclature		Ω	Degree of reaction
A	Heat transfer area (m^2)	**Subscripts**	
C	Condenser	0	Environment
c	Absolute velocity ($m\ s^{-1}$)	1	Rotor blade inlet
$\bar{c}$	Ratio of absolute velocity	2	Rotor blade outlet
Cp	Specific heat capacity ($kJ\ kg^{-1}\ K^{-1}$)	B	Exhaust pipe
d	Diameter of condenser (m)	C	Condenser
D	Diameter of ratio (m)	CI	Condenser I
$\overline{D}$	Ratio of wheel diameter	CII	Condenser II
E	Exergy (kW)	CS	Cold seawater
f	Friction loss coefficient	c	Critical
h	Specific enthalpy ($kJ\ kg^{-1}$)	E	Evaporation
H	Heat source	f	Friction loss
m	Mass flow rate ($kg\ s^{-1}$)	g	Gaseous
Nu	Nusselt number	H	Heat source
P	Pressure (MPa)	HP	High-pressure stage
Pr	Prandtl number	i	Inside
Q	Evaporation heat (kW)	id	Ideal
Re	Reynolds number	in	Inlet
T	Temperature (K)	l	Liquid
u	Peripheral velocity ($m\ s^{-1}$)	le	Leakage loss
$\bar{u}$	Ratio of peripheral velocity	LP	Low-pressure stage
U	Heat transfer coefficient ($W\ m^{-2}k^{-1}$)	m	Average
υ	Velocity ($m\ s^{-1}$)	max	Maximum
w	Relative velocity ($m\ s^{-1}$)	min	Minimum
$\overline{w}$	Ratio of relative velocity	net	Net power
W	Power (kW)	o	Outside
x	Vapor quality	P	Pump
ΔT	Temperature difference (K)	s	Isentropic
Greek symbols		t	Turbine
α	Heat transfer coefficient ($W\ m^{-2}\ K^{-1}$)	u	Peripheral
β	Relative velocity angle (°)	w	Wall
θ	Relative velocity angle (°)	WS	Warm seawater
δ	Tip clearance (m)	**Abbreviations**	
γ	Wall thickness (m)	ED	Exergy destruction
λ	Thermal conductivity ($W\ m^{-1}K^{-1}$)	ORC	Organic Rankine cycle
ξ	Loss coefficient	ZO	Zeotropic organic Rankine cycle
η	Efficiency	PMZO	Parallel multi-pressure evaporation zeotropic organic Rankine cycle
μ	Viscosity (Pa s)	SMZO	Series multi-pressure evaporation zeotropic organic Rankine cycle
ρ	Density ($kg\ m^{-3}$)	PMZO-SL	Parallel multi-pressure evaporation zeotropic organic Rankine cycle with single-outlet liquid-separated condenser
τ	Blockage factor	SMZO-SL	Series multi-pressure evaporation zeotropic organic Rankine cycle with single-outlet liquid-separated condenser
φ	nozzle velocity coefficient	PMZO-DL	Parallel multi-pressure evaporation zeotropic organic Rankine cycle

			with dual-outlet liquid-separated condenser
ψ	rotor blade velocity coefficient	SMZO-DL	Series multi-pressure evaporation zeotropic organic Rankine cycle with dual-outlet liquid-separated condenser

Declaration of interests

☒ The authors declare that they have no known competing financial interests or personal relationships that could have appeared to influence the work reported in this paper.

☐The authors declare the following financial interests/personal relationships which may be considered as potential competing interests: